

Revised UV absorption spectra, ozone depletion potentials, and global warming potentials for the ozone-depleting substances CF₂Br₂, CF₂ClBr, and CF₂BrCF₂Br

Dimitrios K. Papanastasiou,^{1,2,5} Nabilah Rontu Carlon,^{1,2} J. Andrew Neuman,^{1,2} Eric L. Fleming,^{3,4} Charles H. Jackman,³ and James B. Burkholder¹

Received 8 November 2012; revised 19 December 2012; accepted 24 December 2012; published 31 January 2013.

[1] The contribution of Halons, bromine-containing haloalkanes, to stratospheric ozone depletion is highly dependent on their atmospheric lifetime, which is primarily determined by UV photolysis. In this work, UV absorption cross-sections of the ozone-depleting substances CF₂Br₂ (Halon-1202), CF₂ClBr (Halon-1211), and CF₂BrCF₂Br (Halon-2402) were measured between 300 and 350 nm over the temperature range 210–296 K using cavity ring-down spectroscopy. Rayleigh scattering cross-sections were also determined and utilized in the cross-section determination. Spectra parameterizations are presented and 2-D atmospheric model calculations were used to determine global annually averaged atmospheric lifetimes of 2.52, 16.4, and 28.3 years, ozone depletion potentials (ODPs) of 1.95, 8.1, and 18.4, global warming potentials (GWPs) of 175, 1940, and 2270 (100-year time horizon), and associated uncertainties for CF₂Br₂, CF₂ClBr, and CF₂BrCF₂Br, respectively. The revised lifetimes, ODPs, and GWPs differ from values currently reported in international assessments to evaluate ozone recovery and climate change. **Citation:** Papanastasiou, D. K., N. R. Carlon, J. A. Neuman, E. L. Fleming, C. H. Jackman, and J. B. Burkholder (2013), Revised UV absorption spectra, ozone depletion potentials, and global warming potentials for the ozone-depleting substances CF₂Br₂, CF₂ClBr, and CF₂BrCF₂Br, *Geophys. Res. Lett.*, 40, 464–469, doi 10.1002/grl.50121.

1. Introduction

[2] Fluorochlorobromocarbons, Halons (haloalkanes), are a class of manmade ozone-depleting substances (ODSs) and, in many cases, potent greenhouse gases (GHGs) [WMO, 2011]. Halons are emitted directly into the

atmosphere and represent a source of stratospheric bromine, which participates in catalytic ozone destruction cycles, important particularly in the lower stratosphere and in polar stratospheric ozone depletion events, where ClO radical abundances are elevated. The Montreal protocol and its amendments have targeted manmade Halons as compounds to be phased out of commercial use due to their potential harmful effects on the ozone layer; as a result, atmospheric bromine from Halons did not increase during 2005–2008 [WMO, 2011]. The current-day stratospheric abundance of bromine is estimated to be ~22 ppt with 8–10 ppt due to Halons [WMO, 2007, 2011]. Thus, accurate knowledge of the atmospheric lifetime, ozone depletion potentials (ODPs), and global warming potentials (GWPs) of Halons is critical for evaluating their contribution to ozone recovery and climate change.

[3] CF₂Br₂ (Halon-1202), CF₂ClBr (Halon-1211), and CF₂BrCF₂Br (Halon-2402) are key ODSs that are removed from the atmosphere predominantly by UV photolysis [Burkholder *et al.*, 1991]. A primary loss process for these compounds is photolysis at wavelengths >290 nm, which occurs in the troposphere, thus reducing the amount of the compound that can be transported to the stratosphere. However, the UV absorption spectra of these ODSs in the wavelength range >290 nm are not currently known as well as desired for atmospheric modeling purposes. For example, the most recent NASA/Jet Propulsion Laboratory (JPL) data evaluation [Sander *et al.*, 2011] assigned a factor of 2 uncertainty to the >290 nm recommended cross-section data. Estimated uncertainties of this magnitude result in correspondingly large uncertainty in calculated atmospheric photolysis rates, local and global lifetimes, ODPs, and GWPs.

[4] In this work, UV absorption cross-sections, $\sigma(\lambda, T)$, of CF₂Br₂ (Halon-1202), CF₂ClBr (Halon-1211), and CF₂BrCF₂Br (Halon-2402) (also referred to as H1202, H1211, and H2402, respectively, herein) were measured between 300 and 350 nm over the atmospherically relevant temperature range 210–296 K using cavity ring-down spectroscopy (CRDS). A wavelength- and temperature-dependent cross-section parameterization was developed using the present work and results from previous studies at shorter wavelengths. The results were used in the Goddard Space Flight Center (GSFC) 2-D atmospheric model [Fleming *et al.*, 2007, 2011] to evaluate their atmospheric lifetimes and thus ODPs and direct GWPs.

2. Experimental Details

[5] Absorption cross-sections, $\sigma(\lambda, T)$, for the Halons in the >290 nm wavelength range are weak and decrease

All Supporting Information may be found in the online version of this article.

¹Earth System Research Laboratory, Chemical Sciences Division, National Oceanic and Atmospheric Administration, Boulder, Colorado, USA.

²Cooperative Institute for Research in Environmental Sciences, University of Colorado, Boulder, Colorado, USA.

³NASA Goddard Space Flight Center, Greenbelt, Maryland, USA.

⁴Science Systems and Applications, Inc, Lanham, Maryland, USA.

⁵Institute of Chemical Engineering and High Temperature Chemical Processes, Foundation for Research and Technology Hellas, Patras, Greece.

Corresponding author: James B. Burkholder, Earth System Research Laboratory, Chemical Sciences Division, National Oceanic and Atmospheric Administration, 325 Broadway, Boulder, CO 80305-3328, USA. (James.B.Burkholder@noaa.gov)

substantially with increasing wavelength; for H1202, $\sigma(\lambda, 296\text{ K})$ decreases ~ 4 orders of magnitude between 300 and 350 nm. Yet, photolysis over this range is important in its atmospheric photolysis. Molecular Rayleigh scattering cross-sections, $\sigma_R(\lambda)$, for the Halons over this wavelength range are on the order of $\sim 1 \times 10^{-24}\text{ cm}^2\text{ molecule}^{-1}$ (as determined in this work), due to the presence of the highly polarizable bromine, and therefore may contribute significantly to the attenuation (transmission) of a probe beam through a Halon sample. An accurate determination of $\sigma(\lambda, T)$, therefore, requires a technique capable of measuring weak attenuation signals, that is, weak absorption, and methods to accurately account for contributions from Rayleigh scattering to signal attenuation. In this work, CRDS was used to measure absorption coefficients, $\alpha(\lambda, T)$, for H1202, H1211, and H2402 between 300 and 350 nm at temperatures in the range 210–296 K. CRDS measurements performed at temperatures $< 296\text{ K}$ covered a more limited wavelength range than at room temperature due primarily to limitations imposed by the combination of Halon vapor pressure and CRDS sensitivity. CRDS measurements were also simultaneously made at 532 nm, using a second online optical cavity, to determine $\sigma_R(532\text{ nm})$, which aided the evaluation of $\sigma_R(300 < \lambda < 350\text{ nm})$. Measurements at 532 nm also established an upper limit to the possible Br_2 impurity level in the Halon samples. The CRDS apparatus is described in greater detail elsewhere [Feierabend *et al.*, 2009], whereas key experimental components and methods are described briefly below.

[6] The absorption coefficient, $\alpha(\lambda)$, in the CRDS measurements was determined from the ring-down time constants, $\tau(\lambda)$ and $\tau_0(\lambda)$, measured with and without the Halon present in the CRDS optical cavity, respectively:

$$\alpha(\lambda) = (\sigma(\lambda, T) + \sigma_R(\lambda)) [\text{Halon}] = \frac{1}{c} \frac{d}{L_{\text{Abs}}} \left(\frac{1}{\tau(\lambda)} - \frac{1}{\tau_0(\lambda)} \right) \quad (1)$$

where d is the cavity path length, L_{Abs} is the path length of the sample, and c is the speed of light. The Rayleigh scattering cross-section is defined as

$$\sigma_R(\lambda) = \frac{32\pi^3}{3\lambda^4 N^2} (n - 1)^2 \quad (2)$$

where N is Loschmidt's number and n is the Halon index of refraction. $\sigma(\lambda) + \sigma_R(\lambda)$ was determined from a linear least-squares fit of $\alpha(\lambda)$ versus [Halon], that is, a Beer's law analysis, for each wavelength and temperature included in this study. $\alpha(532\text{ nm})$ was measured and taken to be a measure of $\sigma_R(532\text{ nm})$, that is, assuming no sample absorption. $\sigma_R(300 < \lambda < 350\text{ nm})$ was calculated using $\sigma_R(532\text{ nm})$ and Equation (2), although in the final analysis $\sigma_R(300 < \lambda < 350\text{ nm})$, was estimated from the measured temperature dependence of $\sigma(\lambda, T)$, that is, $\sigma(>300\text{ nm}, T)$ is highly temperature dependent, whereas $\sigma_R(\lambda)$ is not. The Rayleigh scattering cross-sections obtained in this way were consistent with the extrapolated values but not identical, that is, an extrapolation assuming a λ^{-4} dependence yielded $\sigma_R(300 < \lambda < 350\text{ nm})$ values $\sim 20\text{--}30\%$ less than inferred from the measured temperature dependence.

[7] CRDS mirrors with maximum reflectivity at 308 nm were used for measurements between 300 and 320 nm and

centered at 340 nm for the 325–350 nm range; typical τ_0 values were ~ 1.4 and $\sim 2\ \mu\text{s}$, respectively, for an optical path of 1 m. For the CRDS 532 nm measurements, τ_0 values were $\sim 40\ \mu\text{s}$ for a 1 m optical path. All measurements at 532 nm were performed at room temperature.

[8] The UV CRDS cell temperature was maintained by circulating a temperature-regulated fluid through its jacket. Gases entering the CRDS cell passed through a 15 cm long side arm that was maintained at the cell temperature. The gas temperature was uniform along the cell to within 0.5 K for temperatures $\geq 250\text{ K}$ and to $\sim 1\text{ K}$ for temperatures $\leq 230\text{ K}$. Room temperature experiments were performed under both static and slow gas flow conditions, whereas reduced temperature experiments were performed strictly under slow flow conditions. The temperature-regulated portion of the optical path length was separated from the CRDS mirrors by $\sim 2\text{ mm}$ diameter apertures mounted within the jacketed portion of the cell. The mirrors were purged with a small flow of He bath gas in the flow experiments that prevented the sample gas from entering the warm region. The optical path length, L_{abs} , under flow conditions, was measured using static and flow measurements of the Halons and CF_3I at room temperature to be $67 \pm 1\text{ cm}$ ($d = 94.5 \pm 0.5\text{ cm}$).

[9] At least six different sample concentrations were included for each experiment. The Halon concentration was determined using absolute pressure measurements and the ideal gas law as well as online UV absorption measurements at 253.7 nm under some conditions. Excellent agreement was observed using these methods under all conditions; no Halon loss was observed while flowing through the system. Absolute pressures ranged from 2 to 200 Torr and were measured using calibrated 100 and 1000 Torr capacitance manometers. CF_2Br_2 (Halon-1202), CF_2ClBr (Halon-1211), and $\text{CF}_2\text{BrCF}_2\text{Br}$ (Halon-2402) ($>99\%$) samples were used as supplied. In addition to the CRDS measurements at 532 nm, the Br_2 impurity level in the Halon samples was tested using chemical ionization mass spectrometry [Neuman *et al.*, 2010] and found to be $< 50\text{ ppt}$, a negligible contribution to the UV absorption coefficient measurements.

3. Results and Discussion

[10] The measured $\sigma(\lambda, T)$ values and 2σ absolute uncertainties, including estimated systematic errors, for H1202, H1211, and H2402 are summarized in Table S1 in the Supporting Information and plotted in Figures 1–3. The $\sigma(\lambda, T)$ values decreased with decreasing temperature at all wavelengths, with the relative decrease being largest at the longest wavelengths. The measured $\alpha(\lambda)$ values behaved linearly over a wide range of Halon concentration under both static and flow conditions, that is, obeyed Beer's law at each wavelength.

[11] The uncertainty in the absorption coefficient measurements and accounting for Rayleigh scattering, particularly at the longer wavelengths, primarily determined the overall accuracy of the reported $\sigma(\lambda)$ values. The precision of the absorption coefficient measurements was $\leq 1.5\%$ for H1202, $\leq 2\%$ for H1211, and $\leq 5\%$ for H2402. The Rayleigh scattering cross-section term contributed a wavelength-dependent uncertainty to the determination of $\sigma(\lambda, T)$, being greatest at the longest wavelengths. The CRDS measurements for each molecule extended to wavelengths long

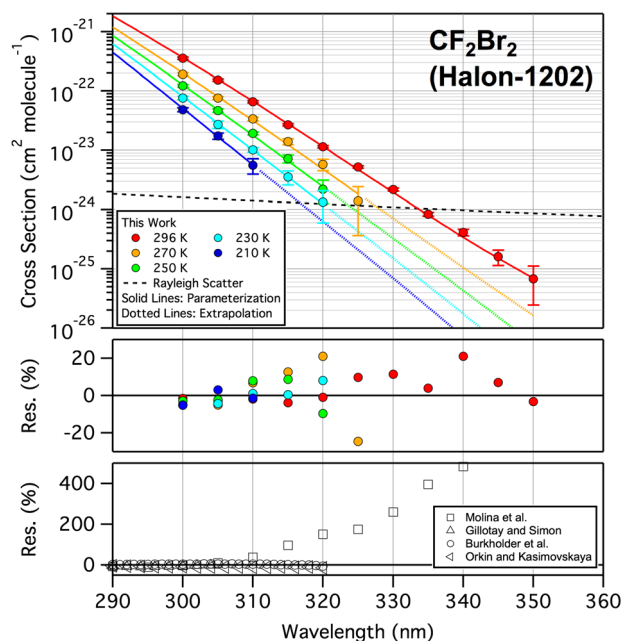


Figure 1. CF_2Br_2 (Halon-1202) UV spectrum. (top) $\sigma(\lambda, T)$ measured in this work (see legend) with 2σ absolute error limits. (middle) Residual for the data obtained in this work. $\text{Res.} = 100 \times (\text{Exp} - \text{Par}) / \text{Par}$. (bottom) Residual for previous room temperature studies.

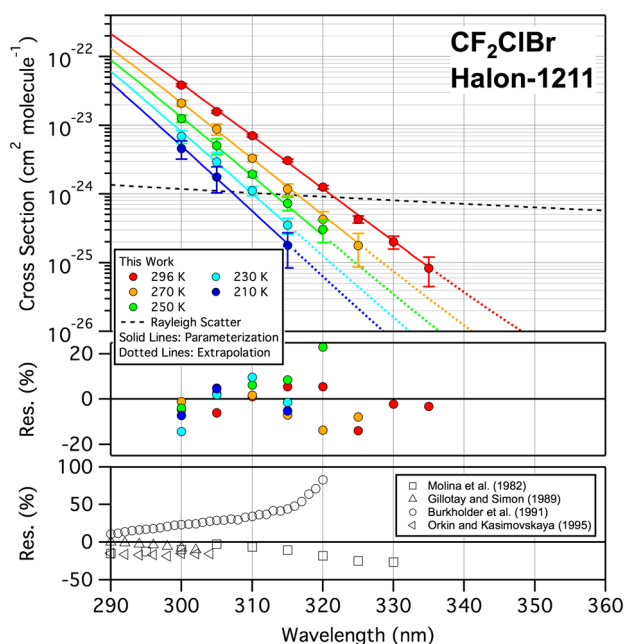


Figure 2. CF_2ClBr (Halon-1211) UV spectrum. (top) $\sigma(\lambda, T)$ measured in this work (see legend) with 2σ absolute error limits. (middle) Residual for the data obtained in this work. $\text{Res.} = 100 \times (\text{Exp} - \text{Par}) / \text{Par}$. (bottom) Residual for previous room temperature studies.

enough that Rayleigh scattering accounted for nearly all of the measured $\alpha(\lambda)$, particularly at reduced temperature, 350 nm for H1202, 340 nm for H1211, and 330 nm for H2402. Thus, $\sigma(\lambda, T)$ obtained at the long-wavelength limit of our

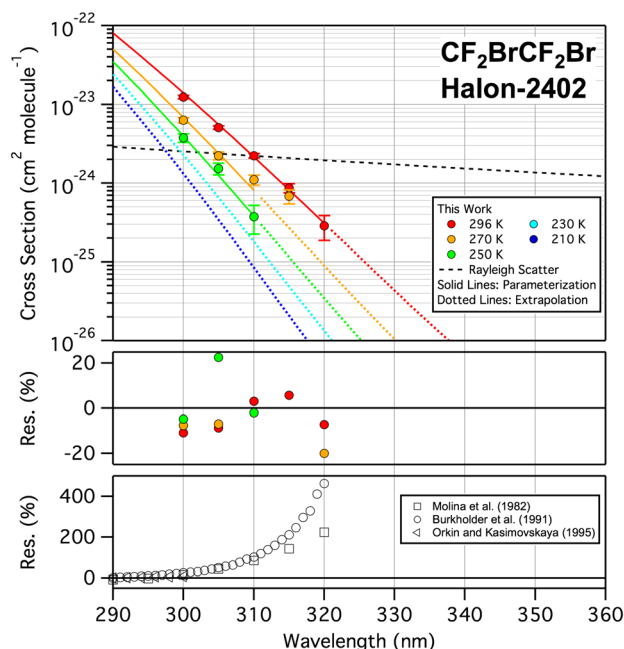


Figure 3. $\text{CF}_2\text{BrCF}_2\text{Br}$ (Halon-2402) UV spectrum. (top) $\sigma(\lambda, T)$ measured in this work (see legend) with 2σ absolute error limits. (middle) Residual for the data obtained in this work. $\text{Res.} = 100 \times (\text{Exp} - \text{Par}) / \text{Par}$. (bottom) Residual for previous room temperature studies.

measurements was highly uncertain and results are not reported in these cases. The Rayleigh scattering contribution decreased substantially toward shorter wavelength where the Halon cross-sections were greater. We estimate that the Rayleigh scattering cross-section at the UV long-wavelength limit of our measurements and the values derived by extrapolating this value to shorter wavelengths (Equation 2) were determined to within $\sim 5\%$. A consideration of measurement uncertainties and accounting for Rayleigh scattering enabled a significant uncertainty reduction in $\sigma(\lambda, T)$ in this work over values reported in previous studies.

3.1. CF_2Br_2 (Halon-1202)

[12] Figure 1 shows the $\sigma(\lambda, T)$ values measured in this work. The $\alpha(\lambda, T)$ values at the longest wavelengths showed no measurable dependence on temperature to within the measurement precision ($\sim 3\%$), and $\sigma_{\text{R}}(350 \text{ nm})$ was determined to be $8.7 \times 10^{-25} \text{ cm}^2 \text{ molecule}^{-1}$. $\sigma_{\text{R}}(\lambda)$ is included in Figure 1 for comparison with $\sigma(\lambda, T)$; $\sigma_{\text{R}}(350 \text{ nm})$ accounted for $\sim 90\%$ of $\alpha(350 \text{ nm}, 296 \text{ K})$ but $< 0.5\%$ at 300 nm. At lower temperatures, the contribution from $\sigma_{\text{R}}(\lambda)$ increased due to the decrease in $\sigma(\lambda, T)$ with decreasing temperature. $\sigma_{\text{R}}(532 \text{ nm})$ was measured to be $(1.24 \pm 0.04) \times 10^{-25} \text{ cm}^2 \text{ molecule}^{-1}$, where the 2σ uncertainty is from the measurement precision.

[13] There are several previous studies of the H1202 UV spectrum to compare with the present work; *Molina et al.* [1982] (190–340 nm, 298 K), *Gillotay and Simon* [1989] (170–304 nm, 210–298 K), *Burkholder et al.* [1991] (190–320 nm, 210–298 K), and *Orkin and Kasimovskaya* [1995] (190–320 nm, 295 K), where the wavelength and temperature range included in the studies are given in parentheses. The differences with the present room temperature results are

shown in Figure 1 (bottom). The agreement is better than ~10%, except for the *Molina et al.* [1982] $\sigma(>305 \text{ nm}, 296 \text{ K})$ values, which are much greater. Note that the literature studies did not account for Rayleigh scattering, which may account for some of the differences. The current NASA/JPL evaluation [*Sander et al.*, 2011] recommends an average of the *Burkholder et al.* [1991] and *Orkin and Kasimovskaya* [1995] results, including an extrapolation for wavelengths $>320 \text{ nm}$.

[14] The temperature dependence of the H1202 UV spectrum was measured previously by *Gillotay and Simon* [1989] and *Burkholder et al.* [1991]. The agreement with the *Gillotay and Simon* study is good for wavelengths $\leq 304 \text{ nm}$. We report a slightly weaker temperature dependence in $\sigma(\lambda, T)$ than reported by *Burkholder et al.*, although the data sets agree to within the combined uncertainty limits for temperatures $\geq 250 \text{ K}$.

3.2. CF₂ClBr (Halon-1211)

[15] Figure 2 shows the $\sigma(\lambda, T)$ values measured in this work. The H1211 UV spectrum at wavelengths $>300 \text{ nm}$ is ~10 times weaker than that of H1202. As a result, the present measurements were limited to wavelengths $<340 \text{ nm}$ and the contribution of Rayleigh scattering is more substantial than for H1202. At 340 nm , the measured $\alpha(\lambda, T)$ values agreed to within ~2% and a $\sigma_{\text{R}}(340 \text{ nm})$ value of $7.2 \times 10^{-25} \text{ cm}^2 \text{ molecule}^{-1}$ was determined. Rayleigh scattering is important at all the wavelengths included in this work; $\sigma_{\text{R}}(300 \text{ nm})$ contributes ~2% to $\alpha(300 \text{ nm}, 296 \text{ K})$ and 20% to $\alpha(300 \text{ nm}, 210 \text{ K})$ (Figure 2). $\sigma_{\text{R}}(532 \text{ nm})$ was measured to be $(9.25 \pm 0.3) \times 10^{-26} \text{ cm}^2 \text{ molecule}^{-1}$, where the 2σ uncertainty is from the measurement precision.

[16] *Molina et al.* [1982] (190–330 nm, 298 K), *Gillotay and Simon* [1989] (170–302 nm, 210–298 K), *Burkholder et al.* [1991] (190–320 nm, 210–296 K), and *Orkin and Kasimovskaya* [1995] (190–304 nm, 295 K) have measured the H1211 UV absorption spectrum previously and the agreement with the present room temperature results is shown in Figure 2. The comparison shows a rather scattered set of data where the discrepancies with the *Burkholder et al.* results are most likely due to the neglect of Rayleigh scattering by *Burkholder et al.* The discrepancies with *Molina et al.* cannot be explained due to their neglect of Rayleigh scattering. The current NASA/JPL evaluation [*Sander et al.*, 2011] recommends an average of the *Molina et al.* and *Burkholder et al.* results extending to 320 nm . The only $\sigma(\lambda, <296 \text{ K})$ data previously available over a wavelength range relevant for long-wavelength atmospheric photolysis was from *Burkholder et al.*, which is superseded by the present work.

3.3. CF₂BrCF₂Br (Halon-2402)

[17] The H2402 UV absorption spectrum is the weakest of the molecules included in this study and Figure 3 shows the $\sigma(\lambda, T)$ values measured in this work. A value of $1.73 \times 10^{-24} \text{ cm}^2 \text{ molecule}^{-1}$ was obtained for $\sigma_{\text{R}}(330 \text{ nm})$ and Rayleigh scattering makes a significant contribution to the measured absorption coefficient for wavelengths $>300 \text{ nm}$ (Figure 3); the contribution at 300 nm is ~20%. $\sigma_{\text{R}}(532 \text{ nm})$ was measured to be $(1.96 \pm 0.04) \times 10^{-25} \text{ cm}^2 \text{ molecule}^{-1}$, where the 2σ uncertainty is from the measurement precision.

[18] Previous studies of the H2402 UV absorption spectrum at $>300 \text{ nm}$ did not account for Rayleigh scattering and are subject to systematic error: *Molina et al.* [1982]

(195–320 nm, 298 K), *Burkholder et al.* [1991] (190–320 nm, 210–296 K), and *Orkin and Kasimovskaya* [1995] (190–300 nm, 295 K). The differences with the present results are large as shown in Figure 3. The present study supersedes the results from *Burkholder et al.* for wavelengths $\geq 300 \text{ nm}$.

[19] In addition to the Halon measurements presented above, $\sigma_{\text{R}}(532 \text{ nm})$ for CF₃Br (Halon-1301) was measured in the course of this work and found to be $(5.1 \pm 0.1) \times 10^{-26} \text{ cm}^2 \text{ molecule}^{-1}$, where the 2σ uncertainty is from the measurement precision. This value is in general agreement with the increasing trend in Rayleigh scattering cross-sections with bromination observed for the other Halons.

[20] $\sigma(\lambda, T)$ was parameterized for use in atmospheric models using the expression given in *Burkholder et al.* [1991]. The equation and fit results are given in Table 1 and included in Figures 1–3 for comparison with the experimental data. The cross-section data from *Burkholder et al.* [1991] was included in the fits for H1202 (260–300 nm), H1211 (206–284 nm), and H2402 (260–280 nm) over the wavelength ranges given in parentheses. The parameterization is considered most valid over the range of the experimental data (see Table S1), whereas extrapolation to lower temperatures seems to yield reasonable values as shown in Figures 1–3. The level of agreement between the parameterization and the data from this study is included in Figures 1–3 (bottom).

4. Atmospheric Implications

[21] The present results were used in the GSFC 2-D atmospheric model to calculate atmospheric photolysis rates as well as local and global annually averaged lifetimes. Details of the model are described elsewhere [*Fleming et al.*, 2007, 2011]. The results are compared with values calculated using the current NASA/JPL [*Sander et al.*, 2011] recommendations. Based on the calculated lifetimes, revised ODPs and direct GWPs (indirect GWPs were not addressed in the present analysis) are reported. The present experimental results not only improve the cross-section database but also significantly reduce the estimated overall uncertainties in $\sigma(\lambda, T)$. The reduced uncertainties obtained in this work have important

Table 1. Parameterization of Absorption Cross-section, $\sigma(\lambda, T)$ (in Units of $\text{cm}^2 \text{ molecule}^{-1}$, base e) Data

$$\ln(\sigma(\lambda, T)) = \sum_i A_i (\lambda - \bar{\lambda})^i \times \left[1 + (296 - T) \sum_i B_i (\lambda - \bar{\lambda})^i \right]$$

Molecule	$\bar{\lambda}$ (nm)	i	A_i	B_i
CF ₂ Br ₂ (Halon-1202)	287.861	0	-47.4178	0.0003173
		1	-0.1567273	1.2323×10^{-5}
		2	-2.624376×10^{-4}	2.68×10^{-8}
		3	-6.78412×10^{-6}	-5.28×10^{-9}
		4	1.261478×10^{-7}	6.99×10^{-11}
CF ₂ ClBr (Halon-1211)	280.376	0	-48.3578	0.0002989
		1	-0.1547325	8.5306×10^{-6}
		2	-4.966942×10^{-4}	4.26×10^{-8}
		3	1.56338×10^{-6}	-1.84×10^{-9}
		4	3.664034×10^{-8}	1.284×10^{-11}
CF ₂ BrCF ₂ Br (Halon-2402)	274.64	0	-48.3611	0.0001877
		1	-0.1595	7.252×10^{-6}
		2	-1.026×10^{-4}	2.917×10^{-7}
		3	-1.334×10^{-5}	-1.725×10^{-9}
		4	1.458×10^{-7}	-2.675×10^{-11}

consequences to the reliability of calculated atmospheric photolysis lifetimes (local and global), ODPs, and GWPs used in assessments and by policy makers. The possible range of these values due to the 2σ uncertainties in experimental parameters was evaluated using the GSFC 2-D model and compared with the NASA/JPL [Sander *et al.*, 2011] recommendations.

[22] Vertical profiles of the global annually averaged photolysis rate coefficient are plotted in Figure 4. The photolysis rate coefficients were broken into contributions from five wavelength regions to illustrate their relative altitude dependent contributions to the local photolysis rate. Photolysis at Lyman- α (121.567 nm) was found to only be important at altitudes >60 km and is not shown in Figure 4; it accounts for $<0.2\%$ of Halon loss. The available $\sigma(<225$

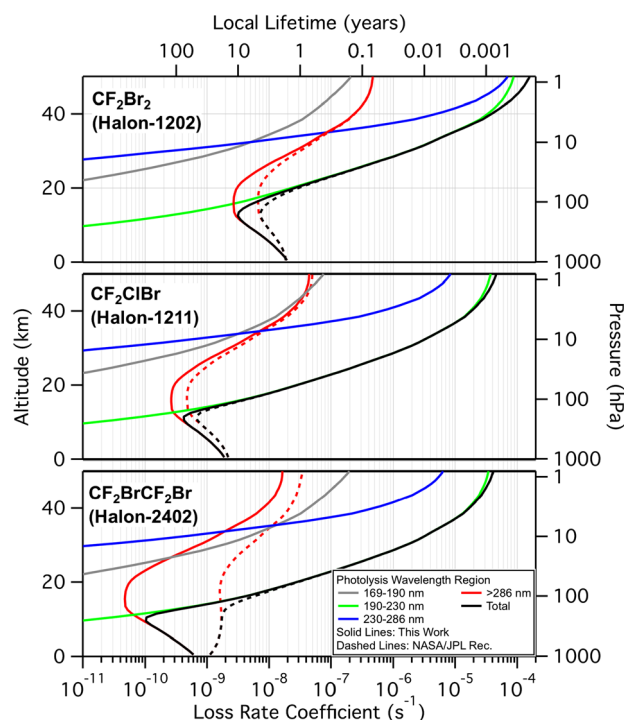


Figure 4. Globally annually averaged atmospheric photolysis loss (local lifetime) profiles for CF_2Br_2 (Halon-1202), CF_2ClBr (Halon-1211), and $\text{CF}_2\text{BrCF}_2\text{Br}$ (Halon-2402) calculated using the GSFC 2-D model. Photolytic loss is separated into four key wavelength regions: 169–190, 190–230, 230–286, and >286 nm (see legend). Calculations were performed using the present results (solid lines) as well as the NASA/JPL [Sander *et al.*, 2011] (dashed lines) recommendations for comparison.

nm,T) data have been reviewed by Sander *et al.* [2011] and the spread in reported $\sigma(\lambda,296\text{ K})$ data is $\sim 10\%$ to 20% between 200 and 225 nm. Resolving discrepancies in this region is desirable to further reduce uncertainties in the calculated Halon lifetimes but was beyond the scope of the present work. The fraction of photolysis in the >290 nm region is most important for H1202 (Table 2), where photolysis at wavelengths <330 nm accounts for $>95\%$ of the long-wavelength photolysis. The global annually averaged lifetimes are given in Table 2. Figure 4 and Table 2 also contain the model results obtained using the NASA/JPL recommended cross-section data for comparison. For each molecule, the calculated tropospheric-lower stratospheric local lifetimes obtained using the present results was greater than obtained using the current NASA/JPL recommendations, with the difference being greatest for H2402; the total global lifetimes given in Table 2 reflect these differences. The range in atmospheric lifetime calculated using the 2σ estimated limits in the cross-section data are also included in Table 2. For the calculations, the 2σ uncertainty factors, $p(298\text{ K})/w$, for $\sigma(\lambda,T)$ were taken to be 1.10/120, 1.10/170, and 1.15/230 for H1202, H1211, and H2402, respectively, where the uncertainty at temperature T is given by $p(T) = p(298\text{ K}) \times \exp(w(1/T - 1/298))$. The lifetime range using the present results are 15%, 16%, and 47% compared with a range of 190–280% obtained using the NASA/JPL uncertainty recommendations, that is, the present results have significantly reduced the estimated uncertainty in the calculated atmospheric lifetimes.

[23] The semiempirical ODPs and the 100-year time horizon GWPs for H1202, H1211, and H2402 were calculated using the methods outlined in WMO [2011] to be 1.95, 8.1, and 18.4 and 175, 1940, and 2270, respectively (Table 2); these values differ from the previously recommended values of 1.7, 7.9, and 13 and 270, 1890, and 1640 cited in WMO [2011] and reported by Orkin *et al.* [2003] for the GWP of H1202 using a 3.9-year lifetime.

[24] In conclusion, the reduced uncertainty in the UV absorption cross-sections reported in this work has led to more reliable estimates of the lifetimes, ODPs, and GWPs for these molecules and these results can be used in future ozone and climate-change assessments. The possible lifetime range, and thus ODP and GWP metrics, was evaluated (Table 2) by including realistic estimated uncertainties in the 2-D model input parameters. This general method of uncertainty analysis can be applied to other ODSs and GHGs addressed in data evaluations and assessments of ozone recovery and climate change.

Table 2. Photolytic Loss, Atmospheric Lifetimes, and Range in Lifetimes Calculated Using the GSFC 2-D Model, ODPs, and GWPs

	Fractional Photolytic Loss ^a		Lifetime (Estimated Range; Range %), ^b (yr)			ODP ^c	GWP ^d
	(<230 nm)	(>286 nm)	WMO [2011]	NASA/JPL ^e	This Work	This Work	This Work
CF_2Br_2 (Halon-1202)	0.056	0.944	2.9	2.08 (0.5–7.5; 280)	2.52 (2.2–2.9; 15)	1.95 (1.7–2.2)	175 (150–200)
CF_2ClBr (Halon-1211)	0.411	0.589	16	13.5 (4.2–34; 190)	16.4 (12.6–20.6; 47)	8.1 (6.2–10.2)	1940 (1320–2810)
$\text{CF}_2\text{BrCF}_2\text{Br}$ (Halon-2402)	0.720	0.280	20	14.1 (4.4–37; 195)	28.3 (24.2–32.9; 16)	18.4 (15.7–21.4)	2270 (1980–2580)

^aGlobal and vertically integrated averages.

^bLifetimes include minor atmospheric loss due to $\text{O}(^1\text{D})$ and OH radical reactions; $<2\%$ of total loss for Halon-1202 and $<0.5\%$ for Halon-1211 and Halon-2402.

^cSemiempirical defined in WMO [2011]. The range in ODP is given in parentheses.

^dValues scaled for differences in lifetime for the 100-year time horizon. The range in GWP is given in parentheses.

^eCalculated using NASA/JPL [Sander *et al.*, 2011] recommendations.

[25] **Acknowledgments.** This work was supported in part by the National Oceanic and Atmospheric Administration Climate Goal Program and the NASA Atmospheric Composition Program.

References

- Burkholder, J. B., R. R. Wilson, T. Gierczak, R. Talukdar, S. A. McKeen, J. J. Orlando, G. L. Vaghjiani, and A. R. Ravishankara (1991), Atmospheric fate of CF_3Br , CF_2Br_2 , CF_2ClBr , and $\text{CF}_2\text{BrCF}_2\text{Br}$, *J. Geophys. Res.*, *96*, 5025–5043.
- Feierabend, K. J., J. E. Flad, S. S. Brown, and J. B. Burkholder (2009), HCO quantum yields in the photolysis of HC(O)C(O)H (Glyoxal) between 290 and 420 nm, *J. Phys. Chem. A*, *113*, 7784–7794.
- Fleming, E. L., C. H. Jackman, D. K. Weisenstein, and M. K. W. Ko (2007), The impact of interannual variability on multidecadal total ozone simulations, *J. Geophys. Res.*, *112*, D10310.
- Fleming, E. L., C. H. Jackman, R. S. Stolarski, and A. R. Douglas (2011), A model study of the impact of source gas changes on the stratosphere for 1850–2100, *Atmos. Chem. Phys.*, *11*, 8515–8541.
- Gillotay, D., and P. C. Simon (1989), Ultraviolet Absorption Spectrum of Trifluoro-Bromo-Methane, Difluoro-Dibromo-Methane and Difluoro-Bromo-Chloro-Methane in the Vapor Phase, *J. Atmos. Chem.*, *8*, 41–62.
- Molina, L. T., M. J. Molina, and F. S. Rowland (1982), Ultraviolet absorption cross sections of several brominated methanes and ethanes of atmospheric interest, *J. Phys. Chem.*, *86*, 2672–2676.
- Neuman, J. A., J. B. Nowak, L. G. Huey, J. B. Burkholder, J. E. Dibb, J. S. Holloway, J. Liao, J. Peischl, J. M. Roberts, T. B. Ryerson, E. Scheuer, H. Stark, R. E. Stickel, D. J. Tanner, and A. Weinheimer (2010), Bromine measurements in ozone depleted air over the Arctic Ocean, *Atmos. Chem. Phys.*, *10*, 6503–6514.
- Orkin, V. L., and E. E. Kasimovskaya (1995), Ultraviolet absorption spectra of some Br-containing haloalkanes, *J. Atmos. Chem.*, *21*, 1–11.
- Orkin, V. L., A. G. Guschin, I. K. Larin, R. E. Huie, and M. J. Kurylo (2003), Measurements of the infrared cross-sections of haloalkanes and their use in a simplified calculational approach for estimating direct global warming potentials, *J. of Photochem. Photobiol., A: Chem.*, *157*, 211–222.
- Sander, S. P., J. Abbatt, J. R. Barker, J. B. Burkholder, R. R. Friedl, D. M. Golden, R. E. Huie, C. E. Kolb, M. J. Kurylo, G. K. Moortgat, V. L. Orkin, and P. H. Wine (2011), Jet Propulsion Laboratory, California Institute of Technology, Chemical Kinetics and Photochemical Data for Use in Atmospheric Studies, Evaluation Number 17, Pasadena, California.
- WMO, (World Meteorological Organization) (2007), Scientific Assessment of Ozone Depletion: 2006, Global Ozone Research and Monitoring Project-Report No. 50, Geneva, Switzerland, 572 pp.
- WMO, (World Meteorological Organization) (2011), Scientific Assessment of Ozone Depletion: 2010, Global Ozone Research and Monitoring Project-Report No. 52, Geneva, Switzerland, 516 pp.